Synthesis and Characterization of Ni–P-CNT's Nanocomposite Film for MEMS Applications

Guang-Ren Shen, Yu-Ting Cheng, *Member, IEEE*, and Li-Nuan Tsai

***Abstract*—An electroless phosphorus nickel–carbon nanotube's (Ni–P-CNT) nanocomposite film synthesis and related process for microelectromechanical systems device fabrication have been successfully developed and presented in this paper. With a special acid oxidative method, a well-dispersed nickel-CNT's colloidal solution has been produced without any aggregation, which is very suitable for microstructure fabrication. The nanoindentation measurement indicates that the Young's modulus and hardness of the Ni–P-CNT's nanocomposite film plated in the bath with 0.028-g/L CNTs can greatly increase up to 665.9 and 28.9 GPa, respectively, which are approximately four times larger than that of pure nickel. Moreover, the content of CNTs in the Ni–P-CNT's films is measured by an elemental analyzer. Via the electrical resistivity measurement using a four-point probe, it is found that the electrical property of the nanocomposite film can be well characterized using a Maxwell–Wagner model for a two-phase mixture. The performance improvements of the electrothermal microactuator made of the nanocomposite, including device strength and power efficiency, have been proven similar to the actuator made of the Ni-diamond composites by electrolytic plating by Tsai *et al.*, but with more efficiency and higher strength than the Ni-diamond device does.**

***Index Terms*—Carbon nanotube (CNT), electroless plating, electrothermal microactuator, nanocomposite, nickel.**

I. Introduction

RECENT technology advancement in material synthesis facilitates the fabrication of nanocomposite materials. A variety of metal/ceramic nanocomposites [1]–[5] have been successfully developed and characterized for many potential applications ranging from tribological coating, RF microelectromechanical systems (MEMS), to data storage system fabrications. Via the second phase enhancement and size effects [6], [7], a metal incorporated with well-dispersed ceramic nanopowders like Al_2O_3, Si_3N_4, SiC, diamond, and Fe (II, III) oxide can have superior homogeneously physical and mechanical properties including the augments of hardness, Young's modulus, fracture strength, and relative permeability (μ_r) that are beyond the intrinsic characteristic limits of the metal. Such a composite can provide an alternative choice of the structure material for MEMS fabrication. Thus far, the nanocomposites can be synthesized using sol gel, co-sputtering, co-milling and hot-pressing, or electrodeposition techniques. However, among these methods, the electrodeposition technique is a cost-effective CMOS compatible process, which can produce thin nanocomposite films under a low processing temperature environment ($<$100 °C) and makes itself very suitable for integrated nano/microelectromechanical systems (N/MEMS) fabrication. In addition, Seung *et al.* designed and fabricated a useful structure composed primarily of electroless nickel. The structure contains a large-area suspended layer and can be easily sealed to form a gas-tight cavity [8] for protective cavities, reservoirs, attachment surfaces, back plates, and mechanical diaphragms application. Chad *et al.* utilized electroplating and electroless nickel to fabricate a micro-cross-flow heat exchanger with good cooling performance [9].

Previously, we have developed a selective electrodeposition process of nanocomposites for MEMS fabrication [10]. Based on the technique, an electrothermal actuator made of Ni-diamond nanocomposite material [1] was successfully fabricated and demonstrated with excellent mechanical strength and power-efficient performance, which is very suitable for low-power microsystem applications. Meanwhile, Chen *et al.* [11] have found the wear rate and friction coefficient of the phosphorus nickel–carbon nanotube (Ni–P-CNT) can be substantially reduced due to the hardness improvement and the unique topological structure of the hollow nanotubes. Inasmuch as the CNT has a higher Young's modulus ($>$1.8 TPa) and bending strength ($\sim$14.2 GPa) [12] than the nanodiamond powder has and the fibrous structure of CNT is different from the diamond shape, the strengthening effects using the Ni–P-CNTs on the device performance could be very different in comparison with the Ni-diamond nanocomposite film. Moreover, CNTs always congregate in a water-based solution due to their nonpolarized surface characteristic and fiber shape so they cannot be separated using ultrasonication. The agglomeration makes the tubes not appropriate for the MEMS device fabrication. Thus, unlike the previous Ni-diamond plating bath [1], in this paper, we will present a novel electroless Ni–P-CNT's plating process for MEMS fabrication and a first fabricated electrothermal microactuator with nanocomposite strengthening effect.

II. Fabraction Process

A. Ni–P-CNT's Plating Solution Preparation

In the experiment, multiwalled CNTs (OD: 10–20 nm, ID: 5–10 nm, length: 0.5–200 μm and bulk density:

Manuscript received July 9, 2004; revised February 12, 2005. This work was supported by the National Science Council, R.O.C. under Grant NSC 92-2220-E-009-006 and in part by the MediaTek Research Center.

G.-R. Shen was with the Microsystems Integration Laboratory, Department of Electronics Engineering, National Chiao Tung University, Taiwan 300, R.O.C. He is now with BenQ, Hsinchu, Taiwan 300, R.O.C.

Y.-T. Cheng is with the Microsystems Integration Laboratory, Department of Electronics Engineering, National Chiao Tung University, Taiwan 300, R.O.C. (e-mail: ytcheng@mail.nctu.edu.tw).

L.-N. Tsai is with the Microsystems Integration Laboratory, Department of Electronics Engineering and Department of Mechanical Engineering, National Chiao Tung University, Taiwan 300, R.O.C.

Digital Object Identifier 10.1109/TNANO.2005.851397

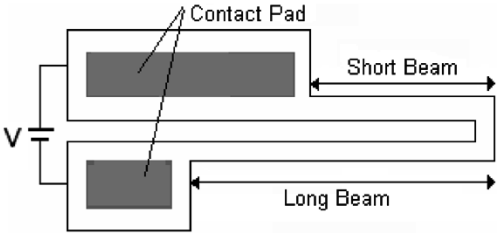

Fig. 1. Schematic diagram of the long–short-beam electrothermal microactuator [15].

0.04–0.05 g/cm^3) are chosen for the synthesis of Ni–P-CNT nanocomposites. The acid oxidative method [13] is utilized to modify the surface chemistry of the CNTs that can make the nanotubes well dispersed within the water. The preparation of the Ni–P-CNT's plating solution is the following. At first, the CNTs are added into an acidic solution of 30-mL H_2SO_4 and 20-mL H_2O_2 combination to form the carboxylate COO^- groups on the sites of the defects and ends of the tubes. Such a treatment can effectively prevent the self-curl phenomenon and the aggregation between these tubes and make the tubes well disperse within the plating bath. The CNTs will still retain their van Hove singularities after the oxidative treatment [14]. After that, the acidic solution is sonicated for 30 min to keep the CNTs separating more uniformly and to form an acidic colloidal solution with a negative pH value. Subsequently, the CNT's colloidal solution is mixed with a commercial Ni–P plating solution. Since most of Ni–P plating solution is well functional around the pH value of 4.5, D.I. water and NH_4OH for the neutralization are then added to form a total volume of 1 L of the Ni-CNT's plating solution. It is noted that the NH_4OH combined with the residual H_2O_2 in the acidic CNT's solution will chemically react with Cu, which results in the disappearance of the seed layer on the wafer and makes the plating process fail. Hence, the acidic CNT's solution is distilled at 250° to fully decompose the residual H_2O_2 into H $_2$O and O_2 before being added into the commercial nickel-plating bath.

B. Design and Fabrication of the Electrothermal Microactuator

The electrothermal microactuator is based on the long-short beam design [15], as shown in Fig. 1, which consists of a pair of adjacent cantilever beams with different lengths that are connected in one end. By applying an electric current through the contact anchors to electrically heat the two beams, the tip of the beams curls toward the shorter one due to the unequal thermal expansions of the two beams. In the design, the length ratio of the long beam to the short one is 2 and the length of the longer beam is 800 μm. Both beams are 10-μm wide and 9-μm thick. The gap between these two beams is 10 μm.

For the electrothermal microactuator fabrication, as shown in Fig. 2, a 2-μm high-density plasma-CVD (HDP-CVD) SiO_2 as the electrical insulation and sacrificial layer is firstly grown on a 4-in silicon wafer after the standard RCA clean. A seed layer of Ti/Cu (100 Å/500 Å) is then sputtered on the top of the SiO_2 followed by a 10-μm-thick AZP-4620 photoresist deposition that is patterned as the device mold of the actuator. Prior to the plating process, the wafer is dipped into a Pd seeding solution

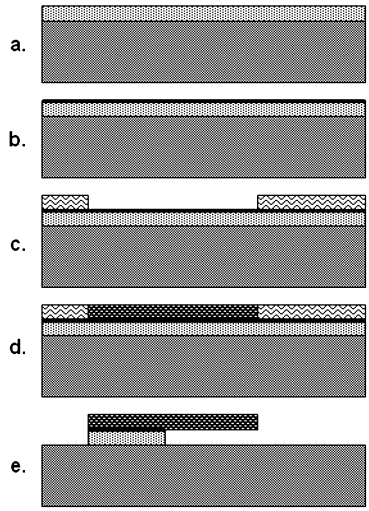

Fig. 2. Process flow of the electrothermal microactuator. (a) 2-μm HDP-CVD SiO_2 for electrical isolation. (b) Ti/Cu (100 Å/500 Å) seed layer deposition. (c) 10-μm-thick AZP-4620 coating and patterning as the plating mold. (d) Electroless deposition of the Ni–P-CNT's nanocomposite for the electrothermal microactuator. (e). Liftoff to release the actuator.

for 30 s to active the copper surface. The Pd solution seeding process is for the purpose of surface chemistry modification of Cu. Pd ions will physically adhere only onto the copper surface and catalyze the redox reaction once the wafer is immersed into the plating bath. After being seeded, the wafer is put into the colloidal plating bath for a 9-μm-thick Ni–P-CNT's nanocomposite film deposition in which the temperature is kept at 78 °C.

Under the environment of ultrasonication and agitation to circulate the plating solution for making the CNT's disperse uniformly, the total plating time is approximately 90 min, which is almost the same as the normal plating time. Once the plating process is done, acetone, and the mixture of an NH_4OH+H_2O_2 solution are then utilized for the removal of the PR mold and the copper seed layer. After the seed layer removal, the wafer is dipped into HF acid to etch away the Ti and SiO_2 sacrificial layer under the beams. An electrothermal microactuator made of Ni–P-CNTs is then fabricated. Fig. 3 shows the scanning electron microscopy (SEM) photograph of the fabricated electrothermal microactuator made of this Ni–P-CNT's nanocomposite material. In front of the tip of the actuator is a scale ruler for the observation of the tip displacement as the device is operated.

III. Characterizations of the Ni–P-CNTs Nanocomposite Films.

A. Composition Analysis and Surface Morphology of the Ni–P-CNT's Nanocomposite

Energy-dispersive spectroscopy (EDS) is utilized for the verification of the CNTs incorporation of the as-plated Ni–P-CNT's nanocomposite. In comparison with the energy spectrum of the plated pure nickel film, as shown in Fig. 4(a), the carbon peak indicates the existence of the CNTs that are embedded in an Ni–P metal matrix, as shown in Fig. 4(b). In order to further verify the carbon signal originating from the CNTs, an X-ray diffractometer, Philips X'Pert Pro (MRD), is utilized to compare the

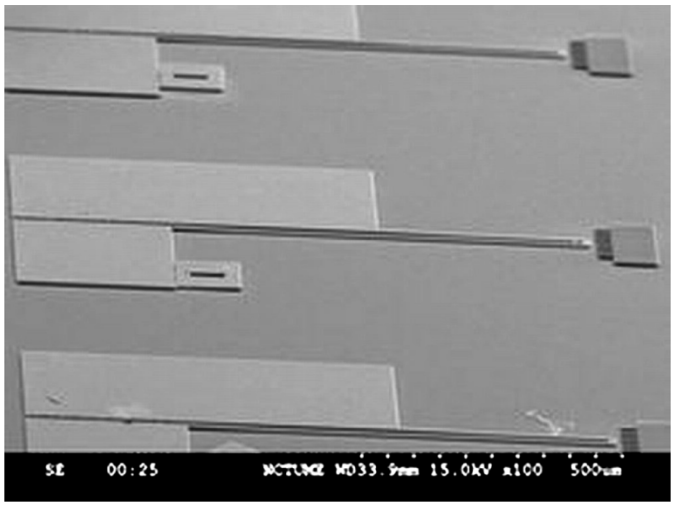

Fig. 3. SEM photography of the as-fabricated Ni–P-CNT's electrothermal microactuator.

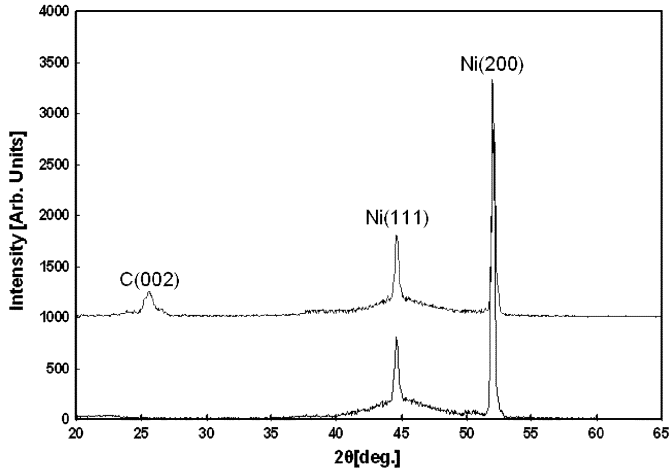

Fig. 5. Superposed XRD diagram of the Ni–P and Ni–P-CNT's films (intensity + 1000 arb. units) indicates the coexistence of the Ni and CNTs.

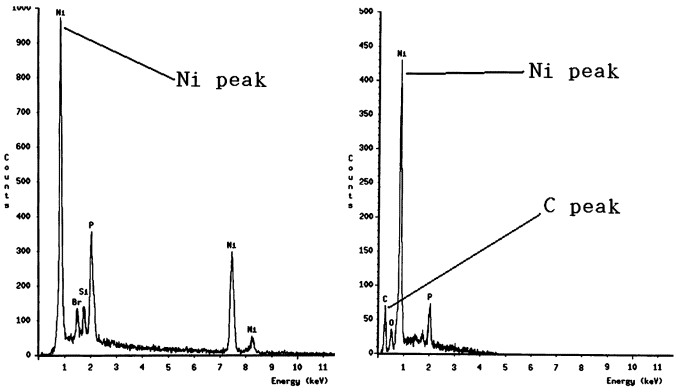

(a) (b)

Fig. 4. EDS spectrums of: (a) the pure Ni–P film and (b) the Ni–P-CNT's nanocomposite film.

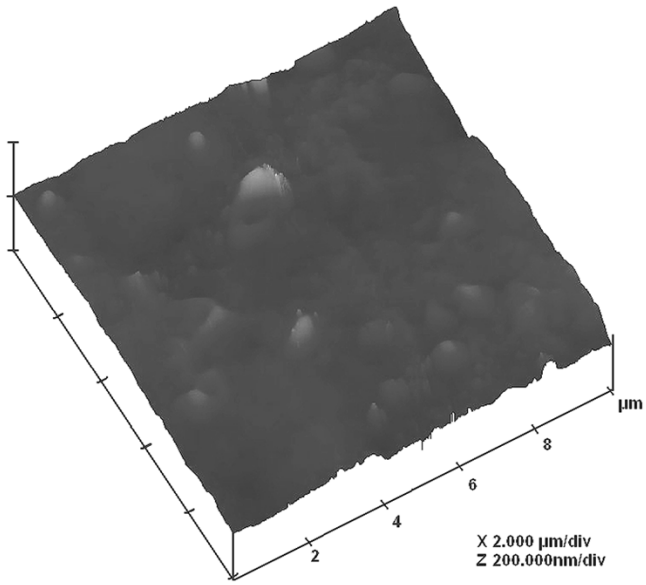

Fig. 6. AFM image of the pure Ni–P film surface morphology.

Ni–P and Ni–P-CNT's nanocomposite films by low-angle X-ray diffraction. The X-ray source is a Cu–kα line with $\lambda = 0.154$ nm. The detection range is made at low angles from $20° < 2\theta < 60°$.

Fig. 5 shows the diffraction pattern of the Ni–P film. The Ni(111) and Ni(200) peaks appear at the angles at approximately 44.8° and 52°, respectively. Meanwhile, the broad bandwidth peak around $2\theta = 45°$ overlapping with the Ni(111) microcrystalline peak also reveals the existence of amorphous Ni phase, which generally appears in as-plated Ni–P film. However, the amorphous phase will disappear and transform into crystalline after the process of high-temperature annealing (>400 °C) [16]. In the XRD spectrum of the Ni–P-CNT's film, the C(002) peak around $2\theta = 26.1°$ indicates that graphite layers are regularly stacked and amorphous carbon exists simultaneously inside the carbon nanotubes. The corresponding carbon interlayer $d_{002} = 3.423$ Å shows that a given interlayer space of the CNT higher than graphite (3.354 Å) can be regarded as the turbostratic stacking of graphitic sheets (neighboring graphitic sheets are parallel to each other, but translational and rotational correlations within a sheet plane are random) [17].

The surface roughness and embedded CNTs on the surface of the composite film are characterized under an atomic force microscope (AFM). As shown in Figs. 6 and 7, respectively, the surface morphology of the pure Ni–P film is different from that of the Ni–P-CNT's film. There is acicular appearance on the Ni–P-CNT's film surface, which is possibly due to the incorporation of CNTs. In addition, the average roughness of the Ni–P-CNT's film is approximately 8.996 nm, which is close to that of 12.628 nm of the Ni–P film.

To characterize the synthesis process of the nanocomposites, the embedded content of CNTs in the Ni–P-CNT's nanocomposite film is obtained via the measurements of an elemental analyzer (EA). The weight fractions of the CNTs in the Ni–P matrix for different plating conditions, which are 0-, 0.007-, 0.014-, and 0.028-g/L CNTs in the baths, respectively, are found to be 0%, 0.075%, 0.11%, and 0.21%. According to the density of nickel (8.908 g/cm^3) and the bulk density of multiwalled CNT

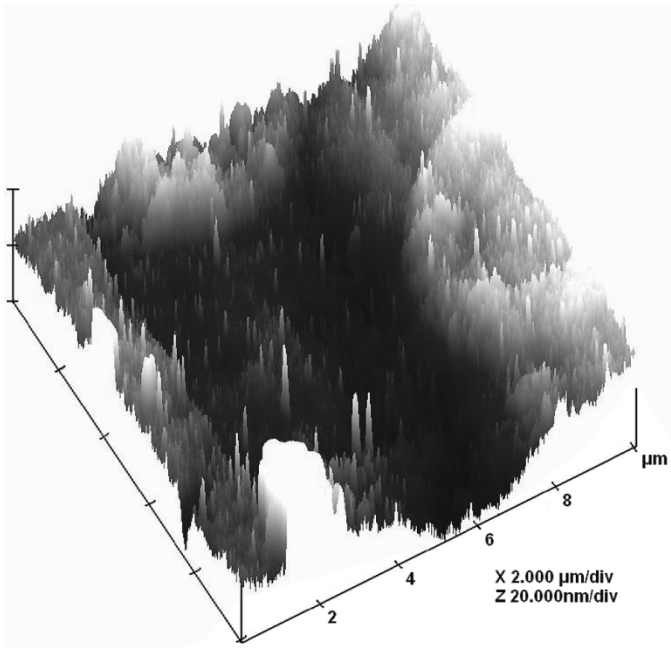

Fig. 7. AFM image of the Ni–P-CNT's composite film surface morphology.

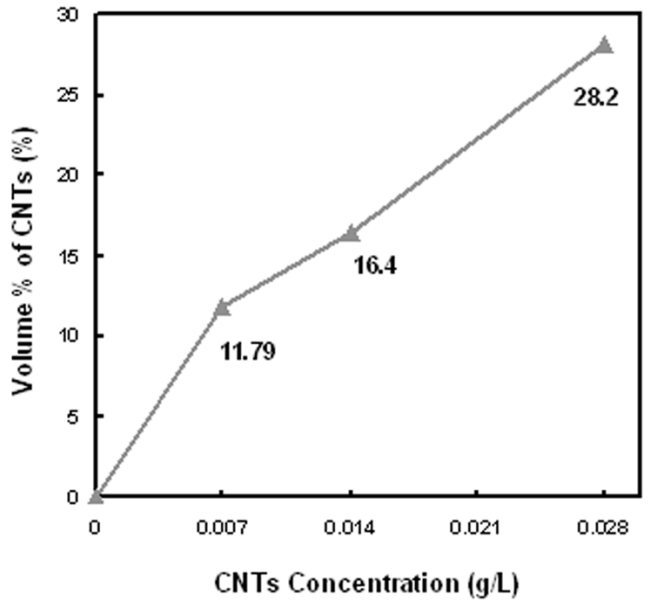

Fig. 8. Volume fractions of the CNTs in the nanocomposite films measured by EA.

(0.05 g/cm^3), the volume fractions of the CNTs is calculated as 0%, 11.79%, 16.4%, and 28.2%, as shown in Fig. 8.

B. Nanoindenter Tests of the Ni–P-CNTi Nanocomposite Film

Fig. 9 shows the results of the nanoindentation tests on four kinds of Ni–P films with different CNT's incorporation. The Young's modului and hardness values are 165.1, 180, 187.2, 665.9, 6.7, 7.3, 8.7, and 28.9 GPa, corresponding to the embedded CNT's concentrations of 0, 11.79, 16.4, and 28.2 vol.%, respectively, in the nanocomposite films. The data shows that slight mechanical strengthening effect is found in the Ni–P-CNT's composite films with 11.79- and 16.4-vol.% CNTs in

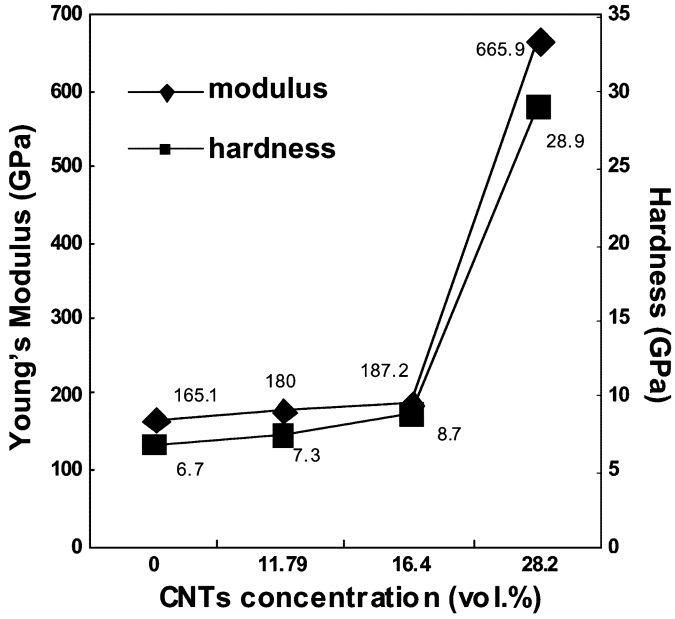

Fig. 9. Nanoindentation test results of the four composite films with different CNT's embedded concentrations, which are 0, 11.79, 16.4, and 28.2 vol.%, respectively.

comparison with the pure nickel film. The Young's modulus and hardness of the films plated in a 0.007- and 0.014-g/L CNT's bath are imperceptible larger than the pure nickel film, except the one plated in the 0.028-g/L CNT's solution. The drastic increase in the 28.2-vol.% CNT's composite film infers that the Young's modulus and hardness of a nickel matrix film can be enhanced up to 665.9 and 28.9 GPa, respectively, which are more than four times of the pure one, while the concentration of the CNTs embedded in the Ni matrix exceeds a threshold value.

C. E/ρ Ratio Analysis

MEMS resonators already revealed high-Q ($>$10 000) and high resonant-frequency characteristics that are feasible in the design and fabrication of high-performance filters and mixers and oscillators [18], [19]. Such resonators are made of polysilicon or polydiamond due to the excellent mechanical properties of high E/ρ ratio (E: Young's modulus, and ρ: density) and low residual stress to the silicon substrate. However, the low deposition rate and high thermal budget of the related processes, which make the resonators hardly integrated with the present CMOS circuitry. While several modular post-CMOS/MEMS integrations have been developed for the co-locating circuits and MEMS [20], these techniques not only demand a high level of precision, but also introduce myriads of other challenges such as bonding, interfacial integrity, and possible damage to movable MEMS components during such endeavors. Therefore, instead of using polysilicon micromachining, the introduction of the nanocomposites in this paper could enable the realization of the final integration of RF MEMS.

In order to further investigate the dynamic performance of the nanocomposites, the cantilever beam arrays made of the Ni–P-CNT's nanocomposites are fabricated with the same plating conditions as the blank nanocomposite film deposition to measure the Young's modulus to density ratio (E/ρ), as shown in

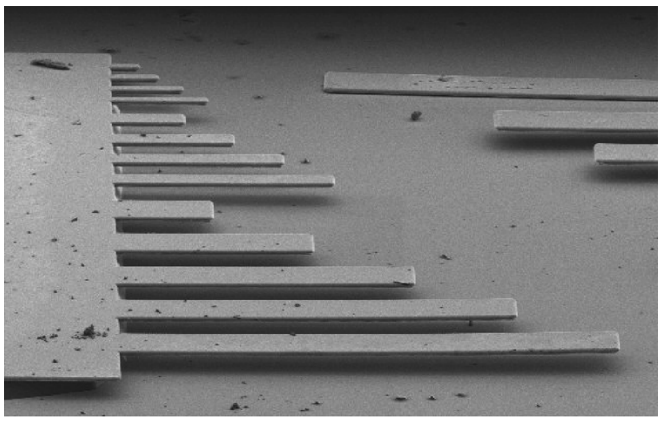

Fig. 10. SEM photograph of the as-fabricated Ni–P-CNT's cantilever beam arrays.

TABLE I
MEASURED RESONANT FREQUENCIES AND THE RELATED DIMENSIONS OF THE SELECTED CANTILEVER BEAMS

	Beam length	Beam thickness	Resonant frequency
Pure Ni	352 μm	8.6μm	24.013kHz
0.007 g/L	358 μm	8μm	24.08kHz
0.014 g/L	358 μm	7μm	32.298kHz
0.028 g/L	358.7μm	7.3μm	38.567kHz

Fig. 10. The fabrication process of the cantilever beams is similar to that of the electrothermal actuator, except the removal of the underneath silicon substrate using TMAH etching for the vertical motion of the device. The laser Doppler vibrometer is utilized for the measurement of the natural resonant frequency of the selected cantilever beam. The resonant frequencies are listed in Table I together with the physical dimensions of the cantilever beams. Based on (1) of the resonant frequency for a standard cantilever beam, the E/ρ ratios are calculated and summarized in Fig. 11. The data shows the E/ρ ratio enhancement of the nanocomposite (28.2-vol.% CNTs) is approximately 3.86 times larger than that of the pure Ni. It reveals the fascination of the nanocomposite for the production of high-frequency microresonators with the low-temperature post-CMOS fabrication process

$$f = 0.1615\frac{h}{L^2}\sqrt{E/\rho} \tag{1}$$

where the symbols are represented as

E Young's modulus of the beam;
ρ density of the beam;
h thickness of the beam;
L length of the beam.

On the other hand, there is another way to evaluate the E/ρ ratio of the nanocomposites. The ratio is obtained by dividing the Young's modulus E from Fig. 9 to the effective density ρ_{eff} of the nanocomposite film derived from (2) of the rule of mixtures [21], [22]. According to the rule of mixtures, the density of a composite material can be approximated as the following relation:

$$\rho_{\text{eff}} = \rho_c f_c + \rho_m f_m \tag{2}$$

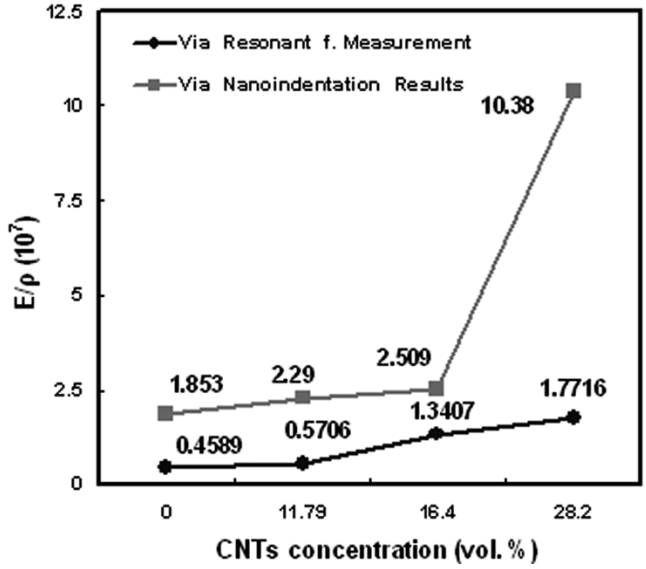

Fig. 11. Comparison of the E/ρ ratios versus CNT's concentrations in the plating baths that were obtained from two different methods.

where ρ_c, f_c, ρ_m, and f_m are the densities and volume fractions of the second phase and composite matrix. Fig. 11 shows the E/ρ ratios of the nanocomposites with different CNT's concentrations derived from this method. In comparison with the ratio calculated from the resonant frequency of the cantilever beam, similar mechanical enhancement trend is found, but with larger E/ρ values.

D. Resistivity Measurement

A four-point probe measurement is utilized to characterize the sheet resistance of the nanocomposite films. Fig. 12 shows that the resistivity is approximately linearly increased with the increasing CNT's concentration due to the contribution of the lower conductivity of CNTs. The conductivity of the multiwalled CNTs is 1.85×10^3 s/cm that is smaller than the pure Ni of 7.964×10^3 s/cm.

E. Device Performance

Fig. 13 shows the measurement results of the electrothermal microactuators made of the nanocomposite films under different plating conditions, which are 0-, 0.007-, 0.014-, and 0.028-g/L CNTs in the baths, respectively. The input power versus displacement data reveals that the performances of the microactuators plated in the baths with 0.007-, 0.014-, and 0.028-g/L CNTs have been improved in terms of the mechanical strength and power efficiency of the device in comparison with that made of pure Ni–P film. The maximum displacement of the actuator made of Ni–P-CNTs (0.028 g/L) can reach 10 μm, which is four times larger than that of the pure one, only with 2.5-μm displacement. Meanwhile, for a 2-μm displacement, the actuator only consumes 0.024 W, which is five times less than that of pure nickel actuator (0.12 W). It shows excellent power improvement, very suitable for low-power microsystem applications. In fact, a similar composite effect has been found in the electroplating Ni/diamond nanocomposite systems [1], but with

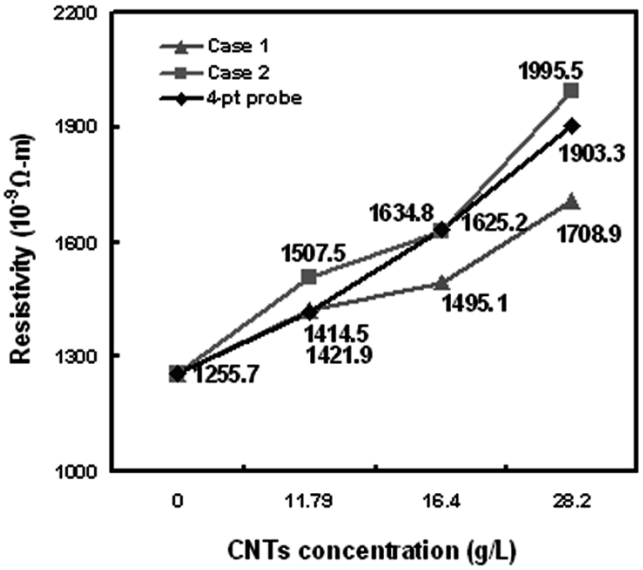

Fig. 12. Comparison of the resistivity values versus different concentrations of CNT's nanocomposite films in the plating solutions. The values are measured by a four-point probe and calculated theoretically using the Maxwell–Wagner two-phase model, respectively.

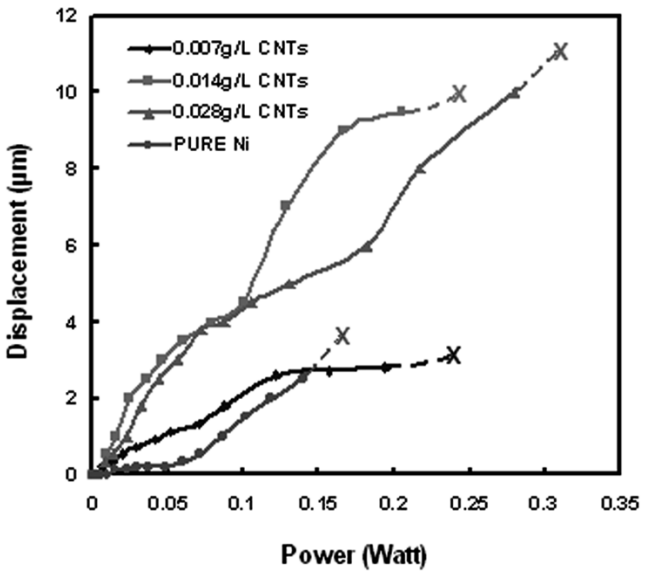

Fig. 13. Measurements of the power versus displacement from Ni–P-CNT's electrothermal microactuators.

better power efficiency (0.16 W) and higher strength than the device made of electrolytic Ni-diamond nanocomposite.

IV. Discussions

The linear rule of mixtures [21], [22] is generally applied to estimate the physical properties of a composite material, such as Young's modulus, hardness, and electrical resistivity, etc. According to the rule, the effective property of the composite has the upper and lower bound values that are approximated as

$$E_{\text{eff}} = E_c f_c + E_m f_m \text{ for the upper-bound}$$
$$E_{\text{eff}} = \frac{E_m E_c}{E_m f_c + E_c f_m} \text{ for the upper-bound}$$

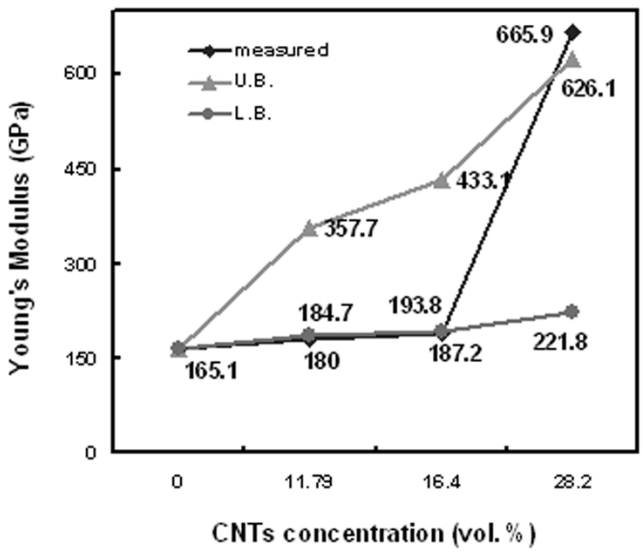

Fig. 14. Comparison of the Young's modului versus different concentrations of CNT's nanocomposite films in the plating solutions. The modului are obtained from nanoindentation measurement and rule of mixtures, respectively.

where E_c, f_c, E_m, and f_m are the physical parameter and the volume fraction of the dopant (CNTs) and matrix (Ni), respectively. Since the Young's modului of Ni and CNT are approximately 165 and 1800 GPa, the upper and lower bounds of the Young's modulus of the Ni–P-CNT's composite can be calculated and plotted in Fig. 14 based on the previous EA analysis. As the embedded CNT's concentration is below 16.4 vol.%, the lower bound model can be applied for the modulus estimation of the composites. In contrast, once the film incorporates 28.2-vol.% CNTs, the upper bound model becomes more applicable. Hence, it is conjectured that there is a critical value of CNT's concentration in the nanocomposite film so that the upper and lower bound models can only be applicable for a certain range while the concentration is higher or lower than the value.

In the measurement of resonant frequency, the selected beam is designed with 350-μm long and 50-μm wide. However, the actual beam length and width measured under optical microscope are not the same as the design due to process variations, as shown in Table I. In addition, the real dimension of the cantilever beam under testing is much larger than that listed in Table I due to the undercut effect. Fig. 15 shows part of the silicon under the beam anchor is etched away during the structure release such that the edge of the anchor pad is freely suspended and the stiffness of the structure is reduced [23]. Therefore, the measured resonant frequency is smaller than expected and it could explain the smaller related E/ρ ratios than the values based on the nanoindentation measurement.

Regarding the electrical characterization of the Ni–P-CNT's nanocomposite films, the measured conductivity of the film can be well estimated using the Maxwell–Wagner equation [24] that is based on the model of a two-phase random network. The conductivity is contributed by the nickel matrix and the embedded CNTs in the films. The Maxwell–Wagner equation is

$$k_c = k_m \frac{1 + 2V_f(1 - k_m/k_d)/(1 + 2k_m/k_d)}{1 - V_f(1 - k_m/k_d)/(1 + 2k_m/k_d)} \qquad (3)$$

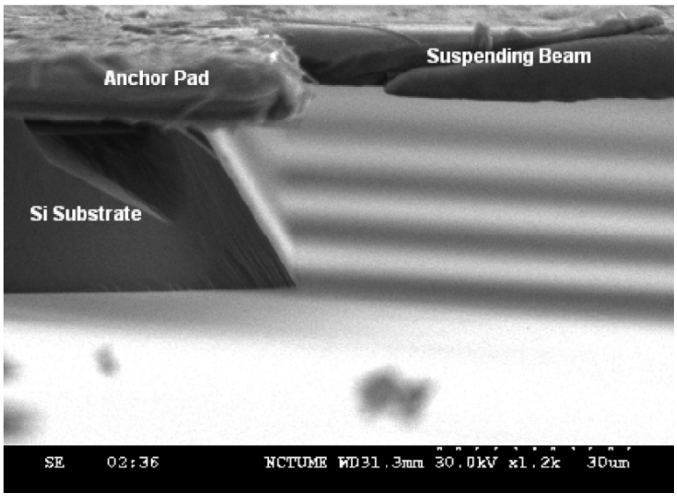

Fig. 15. SEM photograph shows the cross-sectional view of the undercut near the edge of the anchor pad.

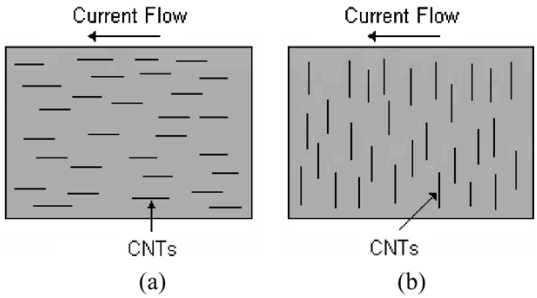

Fig. 16. Two extreme cases of the distributions of the CNTs in the nanocomposite films. (a) Parallel to the current flow. (b) Perpendicular to the current flow.

where V_f is the volume fraction of the second phase and k_c, k_m, and k_d are the conductivities of the composite film, the matrix (Ni), and the second phase (CNTs), respectively. In this model, the assumption of a spherical-shaped second phase is made for the conductivity calculation. However, in this case, CNT utilized here is a multiwalled fibrous structure with one-dimensional (1-D) electrical conduction [25]. The conduction only happens along the longitudinal direction with the 1.85×10^3 s/cm conductivity (k_d). Thus, based on the measured conductivity k_m ($\sim$7.964 $\times$ 10^3 s/cm) of the blank nickel film and previous volume fraction data, it is found that the electrical resistivity of the composite films just falls within two extreme cases correlated with the orientation of the CNT's dispersion, as shown in Fig. 12.

For the first extreme case, it is assumed that the embedded CNTs are oriented along the current flow direction, as shown in Fig. 16(a). The conductivity of the CNTs should be considered and the total conductivity of the composite film is the same as the two-phase Maxwell–Wagner equation. In the second extreme case, the orientation of the embedded CNTs is perpendicular to the direction of current flow, as shown in Fig. 16(b). The CNTs will contribute nil conductivity to the composite film. Therefore, the conductivity of the CNT's k_d can be assumed to be much smaller than that of the Ni matrix k_m. By taking $k_m \gg k_d$ into (3), the Maxwell–Wagner equation is simplified as the following:

$$k_c = k_m(1 - V_f)/(1 + V_f/2). \tag{4}$$

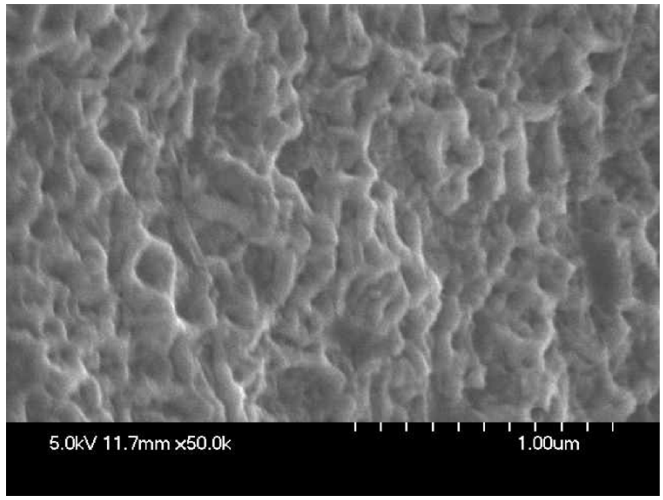

Fig. 17. SEM photograph of the broken interface of the electrothermal actuator made of pure Ni–P film.

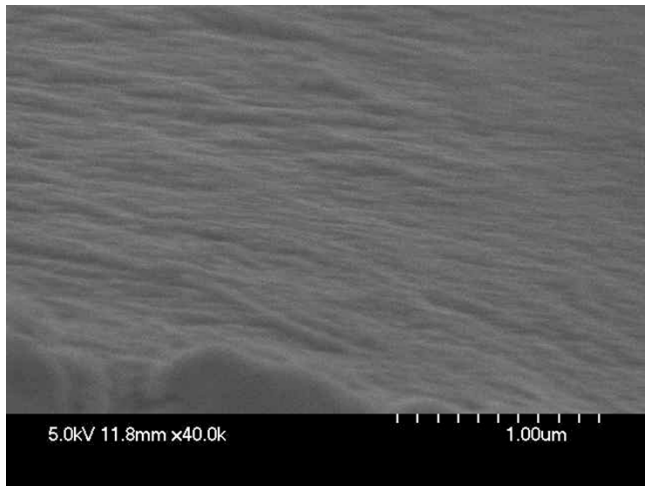

Fig. 18. SEM photograph of the broken interface of the electrothermal actuator made of Ni–P-CNT's nanocomposite (0.014 g/L).

In comparison with the two extreme cases, as shown in Fig. 12, that the resistivity obtained by the four-point probe just falls within two extreme cases means that the distribution of CNTs in the film is in a random dispersion that is all neither parallel, nor perpendicular to the direction of the current flow. The electrical characteristics can be estimated with upper and lower bonds similar to the previous mechanical strengthening effect.

In the experiment, the obvious mechanical strengthening effect is found in the Ni–P-CNT's device instead of the blank film while the incorporated CNTs in the plating bath is below 0.014 g/L. Such a mechanical strengthening effect in the Ni–P-CNT's nanocomposite actuator can be attributed to the molding structure, which would disturb the local hydrodynamic field and result in the increase of the CNT's incorporation. It could also explain why the E/ρ ratios derived from the measurement of the cantilever beam arrays are smaller than we expected due to wider beam width, as described previously. Further investigation is required in the plating process control.

In addition, the broken interfaces of the overloaded actuators have been examined under SEM. Figs. 17 and 18 show that

there are two distinct microstructures existing in the two different devices, which are made of pure Ni–P and Ni–P-CNT's (0.014 g/L) nanocomposite, respectively. Instead of a ductile-type broken interface, as shown in Fig. 17, a brittle-type broken interface is found in the microactuator made of Ni–P-CNTs. The correlation between the mechanical enhancement and the broken interface change due to the incorporation of CNTs is still under investigation.

From (5) of the theoretical calculation for the displacement of the electrothermal microactuators [15], the displacement enhancement of the actuators is correlative to the coefficient of thermal expansion (CTE). Since the conversion factor is only a function of the device geometry, it is speculated that either the CTE of the Ni–P-CNT's nanocomposites material should be larger than the pure Ni–P or the nanocomposite material has lower thermal conductivity than the pure Ni–P such that the microactuator made of the composite performs at higher temperature (larger ΔT), but with the same power input. Research has been conducted to find that the coefficient of the linear thermal expansion increases markedly with the reduction of the average grain size in the Ni–P samples [26]. The related investigations on the CTE and thermal conductivity measurements for the detail are required for future applications of the Ni–P-CNT's nanocomposite

$$\delta = \alpha\left(\gamma_{\text{long}}\Delta T_{\text{long}} - \gamma_{\text{short}}\Delta T_{\text{short}}\right) \tag{5}$$

where δ is the displacement of the beam tip, α is the coefficient of the thermal expansion, $\gamma_{\text{long}}\Delta\gamma_{\text{short}}$ are the conversion factors, and $\Delta T_{\text{long}}\Delta T_{\text{short}}$ are the average temperature changes.

V. Conclusion

The Ni–P-CNT's nanocomposite film and related MEMS devices have been successfully synthesized and fabricated. The incorporation of multiwalled carbon nanotubes (average diameter: 10–20 nm) into the electroless Ni matrix can greatly result in the mechanical property enhancements of the Ni matrix. When the concentration of CNTs embedded in the nickel matrix is over a critical point, the Young's modulus and hardness of the composite film can be increased up to 665.9 and 28.9 GPa, respectively, which are four times larger than that of the pure Ni–P film. Furthermore, based on the measurement of the resonant frequency, the E/ρ ratio of the cantilever beam with 28.2 vol.% CNT's concentration is approximately 3.9 times of the pure Ni one. Such enhancements will be beneficial to microresonant devices for higher frequency performance. Combined with the extraordinary performance including mechanical strength and power efficiency of the electrothermal microactuator made of the Ni–P-CNT's nanocomposite, the nanotechnology shows its potential application for MEMS fabrications.

Acknowledgment

The authors would like to express their appreciations to the Nano Facility Center, National Chiao Tung University, Taiwan, R.O.C., Dr. T. K. Lin, Hwa-Hsia College of Technology and Commerce, Taipai, Taiwan, R.O.C., the group of Prof. W. Hsu, National Chiao Tung University, and C.-J. Shiu and C.-S. Yu, both of the group of Prof. W. Fang, National Tsing Hua University, Hsinchu, Taiwan, R.O.C., for providing technical supports and measurement facilities.

References

[1] L. N. Tsai, G. R. Shen, Y. T. Cheng, and W. Hsu, "Power and reliability improvement of an electro-thermal microactuator using Ni-diamond nanocomposite," presented at the IEEE Electronic Components and Technology Conf., Las Vegas, NV, Jun. 2004, pp. 472–476.

[2] A. F. Zimmermann, G. Palumbo, K. T. Aust, and U. Erb, "Mechanical properties of nickel silicon carbide nanocomposites," *Mater. Sci. Eng.*, vol. A328, pp. 137–146, 2002.

[3] M. Okumiya, Y. Tsunekawa, T. Saida, and R. Ichino, "Creation of high strength bonded abrasive wheel with ultrasonic aided composite plating," *Surface Coatings Technol.*, vol. 169–170, pp. 112–115, 2003.

[4] Y. H. Choa, J. K. Yang, B. H. Kim, Y. K. Jeong, J. S. Lee, T. Nakayama, T. Sekino, and K. Niihara, "Preparation and characterization of metal/ceramic nanoporous nanocomposite powders," *J. Magn. Magn. Mater.*, vol. 266, pp. 12–19, 2003.

[5] C. X. Changrong, X. Guo, F. Li, D. Peng, and G. Meng, "Preparation of asymmetric Ni/ceramic composite membrane by electroless plating," *Colloids and Surfaces A, Physicochem. Eng. Aspects*, vol. 179, pp. 229–235, 2001.

[6] T. Kasagi, "Particle size effect on the complex permeability for permalloy composite materials," *IEEE Trans. Magn.*, vol. 35, no. 5, pp. 3424–3426, Sep. 1999.

[7] L. Carroll, M. Sternitzke, and B. Derby, "Silicon carbide particle size effects in alumina-based nanocomposites," *Acta Mater.*, vol. 44, no. 11, pp. 4543–4552, 1996.

[8] S. H. Yi, F. J. von Preissig, and E. S. Kim, "Electroless nickel films: Properties and fabricated cavity structure," *J. Microelectromech. Syst.*, vol. 11, no. 4, pp. 293–301, Aug. 2002.

[9] C. Harris, K. Kelly, T. Wang, A. McCandless, and S. Motakef, "Fabrication, modeling, and testing of micro-cross-flow heat exchangers," *J. Microelectromech. Syst.*, vol. 11, no. 6, pp. 726–735, Dec. 2002.

[10] K. S. Teh, Y. T. Cheng, and L. Lin, "Nickel nano-composite film for MEMS application," presented at the 12th Int. Solid-State Sensors, Actuators, Microsystems Conf., Boston, MA, June 8–12, 2003.

[11] W. X. Chen, J. P. Tu, H. Y. Gan, Z. D. Xu, Q. G. Wang, J. Y. Lee, Z. L. Liu, and X. B. Zhang, "Electroless preparation and tribological properties of Ni–P–carbon nanotube composite coatings under lubricated condition," *Surface Coatings Technol.*, vol. 160, pp. 68–73, 2002.

[12] E. W. Wong, P. E. Sheehan, and C. M. Lieber, "Nanobeam mechanics: Elasticity, strength, and toughness of nanorods and nanotubes," *Science*, vol. 277, pp. 1971–1975, 1997.

[13] W. Zhao, C. Song, and P. E. Pehrsson, "Water-soluble and optically pH-sensitive single-walled carbon nanotubes from surface modification," *J. Amer. Chem. Soc.*, vol. 124, pp. 12 418–12 419, 2002.

[14] A. G. Rinzler, J. Liu, H. Dai, P. Nikolaev, C. B. Huffman, F. J. Rodríguez-Macías, P. J. Boul, A. H. Lu, D. Heymann, D. T. Colbert, R. S. Lee, J. E. Fischer, A. M. Rao, P. C. Eklund, and R. E. Smalley, "Large-scale purification of single-wall carbon nanotubes: Process, product, and characterization," *Appl. Phys.*, vol. 67, no. 1, pp. 29–37, 1998.

[15] C. S. Pan and W. S. Hsu, "An electro-thermally and laterally driven polysilicon microactuator," *J. Micromech. Microeng.*, vol. 7, pp. 7–13, 1997.

[16] Z. Guo, K. G. Keong, and W. Sha, "Crystallization and phase transformation behavior of electroless nickel phosphous platings during continuous heating," *J. Alloys and Compounds*, vol. 358, pp. 112–119, 2003.

[17] Y. Saito, T. Yoshikawa, S. Bandow, M. Tomita, and T. Hayashi, "Interlayer spacings in carbon nanotubes," *Amer. Phys. Soc.*, vol. 48, no. 3, pp. 1907–1909, 1993.

[18] F. D. Bannon, J. R. Clark, and C. T.-C. Nguyen, "High-Q HF microelectromechanical filters," *IEEE J. Solid.-State Circuits*, vol. 35, no. 4, pp. 512–526, Apr. 2000.

[19] C. T.-C. Nguyen and R. T. Howe, "An integrated CMOS micromechanical resonator high-Q oscillator," *IEEE J. Solid.-State Ciruits*, vol. 34, no. 4, pp. 440–455, Apr. 1999.

[20] K. S. Teh, Y. T. Cheng, and L. Lin, "Nickel nano-composite film for MEMS applications," in *12th Int. Solid-State Sensors Actuators Tech. Dig. Conf.*, Boston, MA, Jun. 2003, pp. 1534–1537.

[21] W. D. Callister, Jr., *Materials Science and Engineering*, 3rd ed. New York: Wiley, 1994, ch. 17, pp. 516–521.

[22] G. E. Dieter, *Mechanical Metallurgy*, 3rd ed. New York: McGraw-Hill, 1978, ch. 6, pp. 184–240.

[23] H. V. Tasi, "Characterization of mechanical properties of thin films using micromachined structures," Ph.D. dissertation, Dept. Power Mech. Eng., Nat. Tsing Hua Univ., Taiwan, R.O.C., 2003.
[24] D. G. Han and G. M. Choi, "Computer simulation of the electrical conductivity of composites: The effect of geometrical arrangement," *Solid-State Ionics*, vol. 106, pp. 71–87, 1998.
[25] Y. Ando, X. Zhao, H. Shimoyama, G. Sakai, and K. Kaneto, "Physical properties of multiwalled carbon nanotubes," *J. Inorganic Mater.*, vol. 1, pp. 77–82, 1999.
[26] K. Lu and M. L. Sui, "Thermal expansion behaviors in nanocrystalline materials with a wide grain size range," *Acta Metall. Mater.*, vol. 43, no. 9, pp. 3325–3332, 1995.

Guang-Ren Shen was born in Taiwan, R.O.C. He received the B.S. degree in physics from National Taiwan Normal University, Taiwan, R.O.C., in 2002, and the M.S. degree in electrical engineering from National Chiao-Tung University, Taiwan, R.O.C., in 2004. His M.S. thesis concerned the synthesis and characterization of Ni–P-CNT's and Ni–P-diamond nanocomposite films for MEMS applications.

He is currently an Engineer with BenQ, Hsinchu, Taiwan, R.O.C., where he is involved with the development of MEMS microfabrication.

Yu-Ting Cheng (M'04) was born in Taiwan, R.O.C. He received the B.S. and M.S. degrees in materials science and engineering from National Tsing Hua University, Hsinchu, Taiwan, R.O.C., in 1991 and 1993, respectively, the M.S. degree in materials science and engineering from Carnegie-Mellon University, Pittsburgh, PA, in 1996, and the Ph.D. degree in electrical engineering from The University of Michigan at Ann Arbor, in 2000. His doctoral dissertation concerned the development of novel vacuum packaging technique for MEMS applications.

Following two-years of army service in Taiwan, R.O.C., he joined Carnegie-Mellon University. Upon graduation, he joined the IBM T. J. Watson Research Center, Yorktown Heights, NY, as a Research Staff Member, where he was involved in several system-on-package (SoP) projects. Since 2002, he has been an Assistant Professor with the Department of Electronics Engineering, National Chiao Tung University, Taiwan, R.O.C. His research interests include the fundamental study of materials for microsystems integration and MEMS applications, SoP, microsensors, and microactuators.

Dr. Cheng is a member of the Institute of Physics (IOP) and Phi Tau Phi.

Li-Nuan Tsai was born in Taiwan, R.O.C. She received the B.S. and M.S. degrees from Da Yeh University, Chang-Hua, Taiwan, R.O.C., in 1999 and 2002, and is currently working toward the Ph.D. degree in mechanical engineering at the National Chiao Tung University, Taiwan, R.O.C.

She is currently involved with MEMS design and fabrication process at National Chiao Tung University.